Super Lyot ExoEarth Coronagraph (SLEEC)

A Technology Development for Exoplanet Missions (TDEM) White Paper

Principal Investigator: John Trauger
Co-Investigators: Pin Chen, John Krist, Dwight Moody

16 March 2018

Jet Propulsion Laboratory
California Institute of Technology

Signature Page

E-SIGNED by John Trauger
on 2018-03-19 11:17:45 GMT

_____

John Trauger Date
PI, SLEEC

E-SIGNED by Brendan Crill
on 2018-03-18 22:54:31 GMT

_____

Brendan Crill Date
Deputy Program Chief Technologist, ExEP

E-SIGNED by Nick Siegler
on 2018-03-18 22:52:57 GMT

_____

Nick Siegler Date
Program Chief Technologist, ExEP

E-SIGNED by Doug Hudgins
on 2018-03-19 22:06:34 GMT

_____

Doug Hudgins Date
Program Scientist, ExEP

1 Objective

The program described herein is a three-year study to include the design, manufacture, and demonstration of coronagraph technology for robust exoplanet imaging and spectroscopic programs with HabEx and LUVOIR. Our objective is to provide enabling coronagraph technologies for the HabEx and LUVOIR mission concepts. The HabEx and LUVOIR objectives include direct imaging and spectroscopic characterization of Earth-like exoplanets in the habitable zones of nearby stars. As detailed in Section 2, these objectives call for coronagraph performance well beyond currently demonstrated capabilities. The SLEEC study includes the design, manufacture, and demonstration of coronagraph technology for robust exoplanet imaging and spectroscopic programs with HabEx and LUVOIR. This work will create realistic (TRL 5) options for space coronagraphs that directly detect and spectrally characterize ExoEarths, and it will provide technical bases and contexts for the HabEx and LUVOIR mission concepts. Our milestone statements clarify these objectives in quantitative form (see Section 3).

2 Introduction/Background

The ongoing HabEx and LUVOIR concept studies have shown that a robust ExoEarth science program requires instrumentation surpassing WFIRST/CGI's pioneering benchmarks. Better contrast, significantly higher core throughput, improved tolerance of telescope pointing jitter and thermal drifts, minimal manufacturing and operational complexity, and larger high-contrast fields of view are among the critical factors.

In pursuit of these performance characteristics, we extend the Lyot coronagraph approach to include the manipulation of wavefront amplitude and phase in all available planes – end-to-end in the coronagraph instrument – leading to "super Lyot" coronagraph systems. This end-to-end systems approach incorporates the following aspects: 1) our best understanding of space telescope performance opportunities and limitations; 2) an optimal coronagraph design with masks and stops at strategic locations in the instrument optical path; and 3) precision wavefront control with state-of-the art deformable mirrors (DMs).

The performance required for enabling HabEx (clear aperture) and LUVOIR's (obscured aperture) scientific goals are roughly an order of magnitude beyond the requirements and expectations for WFIRST/CGI contrast and wavefront error tolerances. We describe below our approach and methodology for achieving the quantitative objectives stated below in Section 3.

2.1 Global Coronagraph Design Approach

Four of the major types of internal coronagraphs (see **Figure 1**) for exoplanet imaging—Lyot, pupil mapping, shaped pupil, and vector vortex—represent, in their classic sense, human choices in starlight-suppression approach with respect to whether it manipulates the wavefront's *amplitude* or *phase* and whether the manipulation occurs in the *pupil* or *image* plane. The shaped pupil coronagraph (SPC) utilizes a binary mask that blocks or transmits light in different parts of the pupil to create dark (high-contrast) regions in the image (Kasdin et al. 2003). The pupil-remapping system, a.k.a. the phase-induced amplitude apodization (PIAA) coronagraph, uses a pair of steeply aspheric mirrors to concentrate and apodize the light toward the center of the coronagraph pupil (Guyon 2003, Belikov et al. 2006). The vector vortex is an image-plane mask that changes the phase of the incoming wavefront to produce a helical phase ramp spanning an even multiple of 2π; the phase

singularity in the vortex's center requires zero amplitude in that region, thereby creating a dark core (Mawet et al. 2010). The Lyot coronagraph utilizes an occulting mask in the image plane to directly block the starlight and a pupil stop downstream to reduce the residual starlight (halo) diffracted by the mask. In particular, the HLC is a modification of the classical Lyot coronagraph; its occulting mask has both a metallic and a dielectric layer to manipulate both the amplitude and phase in the image plane.

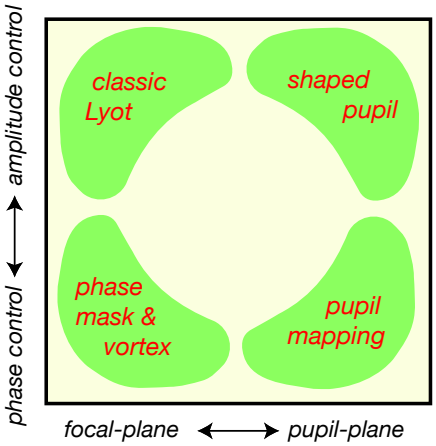

Figure 1. Diagram showing four classic types of coronagraphs for direct detection of exoplanets. The upper-left corner/extreme represents amplitude modification in the focal plane. The upper-right corner represents amplitude modification in the pupil plane. The lower-right corner represents phase modification in the pupil plane. The lower-left corner represents phase modification in the focal plane. The global optimum generally lies somewhere in the middle region, i.e., an amalgamation of all.

In principle, each type can provide complete suppression of monochromatic, unaberrated light in a finite image zone. In practice, they differ in levels of maturity, demonstrated performance (with respect to inner working angle, contrast, throughput, and spectral bandwidth), and sensitivity to disturbances (e.g., line-of-sight jitter and thermally induced telescope aberrations). In the perpetual pursuit of better performance vis-a-vis deleterious pupil architectures and environments, each type of coronagraph has evolved to adopt elements and approaches of other types, blurring the boundaries. For instance, SPC designs for WFIRST now include a focal plane mask and a Lyot stop to form the shaped-pupil Lyot coronagraph (SPLC). PIAA designs evolved to incorporate a diffraction element at a focal plane, giving rise to the PIAA complex mask coronagraph (PIAACMC). A pair of cascaded DMs imbedded in the contemporary HLC act as a pupil re-mapper reminiscent of PIAA (Pueyo & Norman 2013, Mazoyer et al. 2016). Lastly, the vector vortex designs include shaped-pupil or phase-induced remapping to mitigate deleterious aperture effects (Carlotti et al. 2014).

Despite the merging trend of coronagraph architectures and the evident benefits in improving real-world performances, design methodologies are lagging behind the trend. Researchers trained in each school approach the design problem by dynamically optimizing only the element(s) of choice, while using heuristically fixed configuration(s) of the other coronagraph elements. In fact, our team is one of the very few in the practice of jointly optimizing two different categories of coronagraph elements (the two-layer occulting mask and the pair of DMs); nonetheless, we use fixed Lyot-stop geometries and have not incorporated pupil apodization thus far.

The rationale and motivation for a joint optimization approach is as follows. We are dealing with sequential optical planes in a single stream of light; whatever we do upstream affects the optimal design of elements downstream, and vice versa. Therefore, systematically varying/optimizing all the elements is the logical way to find the best overall solution and take full advantage of what a coronagraph can achieve.

In past studies, we have used conventional, gradient-based optimization algorithms. By design, they evolve the state of design parameters such that it descends down a local

valley of objective function surface. As such, incumbent design algorithms do not search for the global optimum, and the obtained solution is particular to the initial state. Except for simple optical systems, these approaches, on their own, may fail to find the global optimum. Finding a global extremum is, in general, a very difficult problem (Press 1992). One standard method is finding local optima starting from widely varying initial states and then picking the best of these; another is simulated annealing, whereby random changes in configuration are introduced during the optimization. Coronagraph designs have not generally utilized these methods. Instead, the user intervenes to heuristically change system specifications and/or mathematical bases to see if a better solution can be found. As the complexity of the system grows, the human-intervention approach becomes increasingly inadequate.

In the present work, we adopt a more holistic design strategy. We augment the gradient-descent algorithm with a MCMC algorithm capable of sampling extraordinarily large parameter spaces to locate the global optimum. Specifically, the MCMC code conducts random walks through parameter space by proposing, at each step, subsequent combinations of DM settings, mask specifications and/or apodizer specifications. Through a process of acceptance/rejection of proposed coronagraph states based on contrast performance and prior constraints, the random walk approaches toward optimum. Our code builds upon the *emcee* program (Foreman-Mackey et al. 2013). As such, we take advantage of *emcee*'s high parallelization efficiency and ability to sample extremely high dimensional space using arbitrarily large numbers of MCMC particles (a.k.a. "walkers"). Indeed, we have successfully conducted simultaneous optimization of 11,000 design parameters, running on only 16 processor cores. At a maximum, we expect our design problems to require optimization of several hundred parameters, and our local cluster furnishes 72 cores at our disposal. Hence, the 11,000-parameter test demonstrates capability far exceeding our requirements using a fraction of our computational resource. The MCMC algorithm usually converges quickly on the approximate optimal solution, yielding the first 2 ~ 3 orders of magnitude improvement in contrast; further performance improvements often progress much more slowly. Therefore, once MCMC finds the approximate global optimum, we use the corresponding state (or a set of states with similar performances) to initialize the gradient-descent software to efficiently deep drill the contrast level. Thus, one can view the MCMC module as a frontend global surveyor augmenting the gradient-descent program. Note that our gradient-descent algorithm has been the state of the art in coronagraph optimization, enabling HLC's recording-holding contrast achievements. The added synergy between MCMC's high-dimensional optimization and the gradient-descent algorithm's refined local optimization is now exploring a new realm of coronagraph design.

As depicted in the flow diagram (**Figure 2**), the design process is initialized with a definition of the optical system including all essential elements from telescope to the final high-contrast science image. The elements to be optimized are modeled in terms of well-chosen basis functions. These take their respective places in the end-to-end system along with the fixed optical elements. The optimization scheme initializes the system with prior knowledge, then guides the optimization with weighted performance criteria (usually a balance of instrument contrast, inner working angle (IWA), tolerance for pointing jitter and low-order aberrations, and overall throughput). Typically, the first phase of the optimization begins with a MCMC exploration of the global parameter space to find the region(s) of convergence.

The solution(s) then feed into our conventional optimization module. The procedure is iterative, in small linear steps in the free parameters with parameter regularization to guide the convergence toward a desired balance of design objectives. A number of design parameters are fixed at the outset and held constant to simplify the optimizations. These fixed trial parameters, which include the radius and circular shape of the focal plane mask (and target IWA), dimensions of the Lyot stop, and spectral bandwidth have been selected on the basis of prior experience and can be either revised in subsequent optimization runs or incorporated into the set of dynamic design parameters. Currently, the procedure includes as free parameters the thickness profiles of the focal plane mask (composed of one nickel and one dielectric layer) and the surface figure settings on each of the two 48 × 48 actuator DMs. Standard multilayer thin film interference code (which generates layer thickness profiles to match specified attenuation and phase profiles) is combined with wavefront control code (which finds the optimal deformable mirror settings)

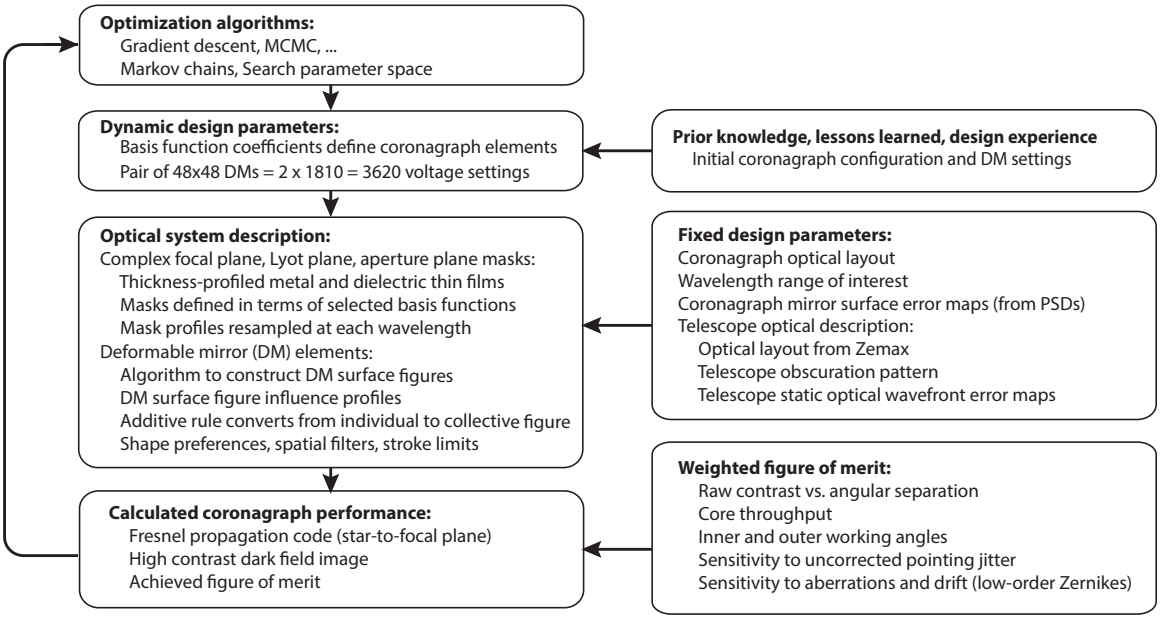

Figure 2. Block diagram of the design optimization process. A set of parameters for the various focal and pupil masks and DM settings conveys the instantaneous state of the coronagraph elements. The process starts with the initial trial design and iteratively adjusts the coronagraph elements to improve the performance, as scored against an objective function. Note that judicious usage of basis functions is key to reducing the dimensionality of the optimization problem, such that a relatively small number of parameters can adequately specify DM actuator setting and mask/apodizer structures.

in an end-to-end optical propagation model. We note that the objective of tolerance to telescope pointing jitter and drift can be "baked into" the design by averaging the effects of multiple low-order zernike wavefront terms (primarily tip/tilt, focus, and astigmatism, as estimated for missions such as HabEx) in each iteration. DM settings are optimized in stages by spatial filtering, progressing from large low-order corrections in the early iterations to small high-order control in the later stages.

Our optical propagation model, based on the Fresnel approximation, incorporates the physical characteristics of the Lyot coronagraph elements, mirror surfaces, the DMs, and the pixel dimensions of the CCD imager. The code is written in Python and has been cross-checked with the publicly distributed PROPER code (Krist 2007), typically showing agreement to within computer rounding errors (Trauger et al. 2016, Trauger et al. 2010). Since the underlying physics is not in question, the accuracy of our model predictions is limited only by the fidelity of our physical descriptions of the critical coronagraph elements (e.g., fabrication errors or insufficient simulation sampling can be fidelity issues). This model has consistently predicted laboratory contrast performance within 15% in prior HCIT (High Contrast Imaging Testbed) demonstrations. The effects of stellar diameter and pointing jitter are idealized in our model as the convolution of a uniform disk for the star (neglecting limb darkening) and a Gaussian-weighted distribution of tip/tilt pointing offsets. The representative target star is given an angular diameter of 1 mas (roughly equal to the angular diameter of the sun at 10 pc). Pointing jitter up to a few milliarcseconds is also incorporated into the process. The presence of these angular offset distributions is represented in our model as a cluster of incoherent point sources with the specified distribution of angular offsets in the sky. The quoted coronagraph contrast is the weighted average of contrasts computed for a large number of representative angular offsets.

2.2 Prolate Spheroidal Basis Functions

A major challenge lies in the dimensionality of the computational problem. For instance, a pair of DMs alone (each with 48 actuators across the diameter) potentially constitutes a 4608-dimensional optimization problem. Conventional optimization approaches involve $O(N^2)$ evaluations, where N is the number of dimensions. In the current fictitious example, this translates to roughly 21 million contrast simulations to find a *local* optimum just for the DMs. Even with highly efficient forward propagation routines and parallel computing, this is a time-consuming exercise; *global* optimization based on conventional methods is practically out of reach.

Utilization of prolate spheroidal wave functions (PSWFs) as basis functions for the design-optimization algorithm is an important part of our innovation. (Note that we use PSWFs as basis sets to represent DM, mask, and apodizer shapes, but we do not use them to represent electric fields.) PSWFs are complete sets of orthonormal basis functions for both finite and infinite domains in both (pupil and image) Fourier spaces. They are the most simultaneously concentrated functions in conjugate Fourier spaces, and they are eigenfunctions of an idealized, zeroth-order coronagraphic problem. Empirically, we have demonstrated their efficiency in reducing dimensionality for our optimization computations. Work by Soummer et al. (2009 and references therein) on optimizing pupil apodization for arbitrary apertures inspired us, although we differ in using PSWFs for reducing dimensionality in joint optimization of multiple planes. PSWFs possess unique properties that enable large reductions in dimensionality and facilitate convergence. To explain its

advantages, we begin by considering the general coronagraph design problem and express the field amplitude in key optical planes as follows:

$$\text{Entrance pupil: } \Psi_1(r) = P(r)\mathrm{K}(r)$$

$$\text{Occulter image: } \Psi_2\left(\frac{\rho}{\lambda f}\right) = \hat{P}\left(\frac{\rho}{\lambda f}\right) * \widehat{\mathrm{K}}\left(\frac{\rho}{\lambda f}\right)\left[1 - A\left(\frac{\rho}{\lambda f}\right)\right]$$

$$\text{Lyot pupil: } \Psi_3(r) = \{P(r)K(r) - \hat{A}(r) * [P(r)K(r)]\}L(r)$$

$$\text{Final image: } \Psi_4\left(\frac{\rho}{\lambda f}\right) = \hat{L}\left(\frac{\rho}{\lambda f}\right) * \hat{P}\left(\frac{\rho}{\lambda f}\right) * \widehat{K}\left(\frac{\rho}{\lambda f}\right) - \hat{L}\left(\frac{\rho}{\lambda f}\right) * \left[A\left(\frac{\rho}{\lambda f}\right)\hat{P}\left(\frac{\rho}{\lambda f}\right) * \widehat{K}\left(\frac{\rho}{\lambda f}\right)\right]$$

Ψ denotes the wavefront amplitude at each plane; $P(r)$ is the aperture transmission function; $K(r)$ is the pupil (apodization) function; the occulter mask's transmission function is expressed as $[1 - A(\rho/\lambda f]$; $L(r)$ describes the Lyot-pupil transmission function; r denotes the position vector in pupil planes; ρ denotes the position vector in image planes; f is focal distance; λ is wavelength; the caret represents Fourier transform; and the asterisk denotes convolution. We will also refer to $A(r)$ as the "occulter opacity function." All of the above quantities are generally complex.

Minimizing Ψ_4 over a domain in ρ creates a dark hole in the final image. Equivalently, we can think of this as minimizing Ψ_3 over an appropriate band of spatial frequencies (since image and pupil amplitudes are Fourier pairs). Note that Ψ_3 consists of destructive interference between the entrance-pupil light and light diffracted by the occulter (and spatially filtered by the Lyot stop). To optimize contrast, occulter absorption function (A) would be such that the convolution $A^*\Psi_1$ ($=A^*PK$) is equal to Ψ_1 itself over the band of interest. The Dirac-delta function would provide an exact solution, but it would also imply an infinitely large occulter (with zero throughput). Ideally, we want image-plane (occulter) basis functions that are the most concentrated in both (image and pupil) Fourier domains to simultaneously optimize contrast and throughput. In addition, orthogonal basis functions forming a complete basis set enables general numerical algorithms to efficiently (due to orthogonality) find global solutions over all possible (due to completeness) occulter functions. Below, we show that PSWFs are such ideal basis functions for constructing arbitrary masks/apodizers in image *and* pupil planes.

Let us consider an idealized 1-D case, where K and L are the same top-hat function with width/diameter d, representing simple apertures, and M is also a top-hat function, representing an opaque occulter. In this case,

$$\Psi_3(r) = K(r) - \int_{-\frac{d}{2}}^{\frac{d}{2}} \frac{sin(r - r')}{\pi(r - r')} K(r')\, dr'$$

We seek $K(r)$ that minimizes Ψ_3.

It turns out that distinguished mathematicians David Slepian, Henry Landau, and Henry Pollak solved the mathematical problem equivalent to this case in the early 1960s, although they did it in the context of a question posed by his Bell Labs colleague Claude Shannon, the father of information theory: To what extent are functions which are confined to a finite bandwidth also concentrated in the time domain? (e.g., Slepian & Pollak 1961, Slepian 1964, 1983). In searching for band-limited functions having the maximum encircled energy within a given spatial domain, this question seeks the ultimate limit to Heisenberg's uncertainty principle. Slepian et al. determined that the solutions are the eigenfunctions of the following eigenvalue problem:

$$\int_{-T/2}^{T/2} \frac{\sin\Omega(t-s)}{\pi(t-s)} \varphi_i(s)ds = \Lambda_i \phi_i(t)$$

The eigenfunction ϕ_0 corresponding to the highest eigenvalue Λ_0 concentrates most encircled energy in *t*. The eigenfunctions are PSWFs. Note that, to within a constant (eigenvalue) factor and trivial changes of variable symbols, we obtain the above equation by setting $\Psi_3 = 0$ in its preceding equation, yielding

$$\int_{-d/2}^{d/2} \frac{sin(r-u)}{\pi(r-u)} A(u)\, du = \Lambda A(r)$$

As Λ approaches unity, Ψ_3 approaches null, yielding optimal contrast (whereas Λ=1 results in the trivial solution of complete blockage of light). The physical interpretation is that the PSWF solution is the pupil apodization concentrating the most starlight onto the occulter mask and thus extinguished (Soummer et al. 2009).

It has been shown that eigenfunctions (generalized PSWFs) can be determined for the 2-D (and higher dimensional) case for arbitrary aperture geometries (Soummer et al. 2009). We see that PSWFs are optimal basis functions for the idealized (zeroth-order) coronagraph problem in image and pupil planes. Different types of aperture geometry give rise to different types of PSWFs, and formal solutions exist in general for any shape of aperture (Soummer et al. 2009, Papoulis 1968). Another unique property is that PSWFs are orthogonal in both Fourier domains over finite and infinite intervals. As such, one can construct an arbitrary function in either domain as a superposition of PSWFs. In addition, the Fourier transform of a PSWF is simply a scaled version of itself. Altogether, being the proper solution to a relevant eigenvalue problem, orthogonality in both pupil and image domains, and shape invariance under Fourier transform can lead to tremendous enhancements in computational efficiency. We have witnessed a factor of 200 reduction in dimensionality compared to using a Fourier (i.e., cosine(x, y)) basis set, thereby improving computational speed by a similar factor.

2.3 Figures of Merit (Objective Function)

Our main objective is to define and demonstrate coronagraph designs capable of exoplanet detection with a specified SNR in a minimum of observing time. Minimum time also works to relax the engineering requirements for long-term telescope and instrument stability. In simplified terms, and neglecting detector noise, the SNR for detection of the planet signal in the presence of astronomical background noise is given by the following equations:

$$SNR^2 = \frac{{\Gamma_{planet}}^2}{\Gamma_{star} + \Gamma_{planet} + \Gamma_{exoZ} + \Gamma_{localZ}}$$

where Γ_{planet}, Γ_{star}, Γ_{exoZ}, and Γ_{localZ}, are (detected) photon counts from the exoplanet, host star, exozodi, and local zodi. We expand this equation in terms of instrumentational/observational parameters:

$$SNR^2 = \frac{(\eta\beta t\varepsilon S)^2}{\eta\beta t(SC + S\varepsilon + SZ_{exo} + Z_{local})} = \frac{\eta\beta t\varepsilon^2 S}{C + \varepsilon + Z_{exo} + \frac{Z_{local}}{S}}$$

where *t* is the integration time, *C* is the instrument contrast ratio (mean speckle background intensity / peak PSF star intensity), η is the instrument core throughput (fraction of PSF energy within the half-peak intensity contour), β is the spectral bandwidth, ε is the

ratio of planet to star brightness, S the spectral photon rate from the star, Z_{exo} is the exozodi photon rate per PSF, and Z_{local} is the photon rate per PSF from local zodi.

Then the integration time to achieve that SNR is as follows:

$$t = \frac{SNR^2\left(C + \varepsilon + Z_{exo} + \frac{Z_{local}}{S}\right)}{\eta\beta\varepsilon^2 S}$$

For the case of negligible (exo- and local-) zodiacal light, this equation simplifies to the following expression:

$$t \cong \frac{SNR^2(C + \varepsilon)}{\eta\beta S\varepsilon^2}$$

We see that instrument contrast C, instrument throughput η, and spectral bandwidth β each influence the integration time directly. The trade between these three critical instrument characteristics will dominate our optimization study. *Therefore, minimization of the integration time (*t*) will be the main objective function for our design optimization.* It is a desirable and important objective because minimal t provides not only greater scientific yield per mission lifetime, but substantial cost savings as well by mitigating stability requirements of an unprecedentedly large space telescope.

Rearranging the preceding equation can yield an informative expression for required contrast as a function of *SNR* and photon count from the planet:

$$\frac{C}{\varepsilon} \cong \frac{\eta\beta t\varepsilon S}{SNR^2} - 1 = \frac{\Gamma_{planet}}{SNR^2} - 1$$

We see that one must detect at least as many photons from the planet as SNR^2 to operate in a realistic contrast realm (i.e., $C \geq 0$). When the planetary photon count is twice SNR^2 (50 photons for $SNR = 5$), the requisite contrast is equal to the planet-to-star brightness ratio. From that point on, increasing the planetary photon count via increases in throughput, bandwidth, or integration time relaxes the contrast requirement proportionally, whereas the radius of the PSF has a quadratic influence on required contrast level. Hence, one must consider contrast requirements in the context of telescope parameters. Our design approach ensures that we aim for optimal coronagraphic designs specific to the evolving HabEx and LUVOIR telescope definitions.

As far as we know, the treatment presented above is new and not in the literature. It is a simple method to incorporate contrast, throughput, and bandwidth in our merit function. It does not narrowly focus on only one or two performance characteristics and is still simple to compute.

3 Milestones Definition

The following milestone statements capture our objectives.

3.1 Milestone 1a (M1a)

Design a Lyot-type coronagraph for a HabEx unobscured off-axis telescope with raw contrast of 10^{-10} or better for spectral bandwidths ≥ 10%, with tolerances to expected levels of telescope jitter and low-order thermal drifts (cf. Table 1). The HabEx project predicts a residual pointing jitter at the coronagraph focal plane of 0.5 milliarcsec rms on each axis (G. Kuan, personal communication, 2018), which will be introduced as a design constraint. Estimates for telescope thermal drift during nominal observing sequences will be incorporated as they become known. Our objective is to maximize the figure-of-merit as

defined in the previous section. This metric is chosen for computational simplicity, as it is embedded in the design optimization loop. Meanwhile, we recognize that by itself this metric does not capture all the performance parameters needed to predict science yields, and note that the exoplanet community continues to refine the relevant science performance metrics. For instance, Bayesian signal detection theory provides a statistical framework for testing the hypothesis of signal present (detection) vs. signal absent (Jensen-Clem et al. 2018). We will periodically check our design performance against these more complete science metrics as we proceed with the design optimization.

3.2 Milestone 1b (M1b)

Using the M1a coronagraph elements on the newly commissioned ExEP Decadal Survey Testbed (DST), demonstrate 10^{-10} contrast, 10% bandwidth in a simulated static vacuum laboratory environment, IWA = 3 λ/D (cf. Crill & Siegler 2017). "Angular separation" is defined in terms of the wavelength λ and the diameter *D* of the aperture stop on the deformable mirror (DM), which is the pupil-defining element of the laboratory coronagraph. We adopt the direct, intuitive, and easy-to-compute definition for contrast per Krist (2016), as has been widely adopted in studies including WFIRST and Exo-C. Contrast for a particular pixel in the field is the ratio of the residual flux at that pixel to the maximum value of the offset stellar PSF. For a set of pixels, such as a dark-hole region or a radial band of pixels at a particular angular separation, the overall contrast is the set's median value.

We note that while the DST is designed as a "static" testbed, it will be possible to test for tolerance to telescope pointing jitter and drift by exercising the Fine/Fast Steering Deformable Mirror (FSDM) element (see Section 4.2).

3.3 Milestone 2a (M2a)

Design a Lyot-type coronagraph for the LUVOIR telescope with a segmented primary mirror configuration, making strategic use of all available design elements at focal planes, pupil planes, and appropriate intermediate planes downstream of the large telescope optics. M2a seeks the best possible exoplanet science performance.

However, the baseline LUVOIR telescope configuration has not been finalized as of the date of this White Paper. Details will include the dimensions and number of mirror segments, the expected optical figure and level of wavefront phase control, and details of the secondary mirror obscurations. Once these have been clarified by the LUVOIR team (likely during the first year of this study), then we will define and submit our M2 performance targets for review and approval by the ExEP office.

3.4 Milestone 2b (M2b)

The manufacture and demonstration of the M2a coronagraph elements on the newly commissioned DST. Expected performance levels will be determined during the design phase of M2a (Table 1 lists notional targets for this phase).

Table 1. State-of-the-Art and Target Coronagraph Performance

Metric	Demonstrated State of the Art		Milestone Demonstrations	
	Clear pupil, lin. mask (Siegler 2016)	**WFIRST obscr. pupil, circ. mask** (Seo et al. 2017)	**Milestone 1b** (clear pupil)	**Milestone 2b** (obscr. pupil) (Patterson et al. 2017)
Raw Contrast	6×10^{-10}	1.6×10^{-9}	$\leq1\times10^{-10}$	$\leq5\times10^{-10}$
Bandwidth	10%	10%	>10%	>10%
Inner Working Angle	3 λ/D	3 λ/D	3 λ/D	3 λ/D

4 Experiment Description

Section 2 details our design methodology, which we utilize for all of our design efforts. Our model for science yield of potential earth-sized exoplanets in the habitable zones of a representative population of nearby stars (including the nearby RV exoplanet targets) will be a metric for scoring coronagraph designs. We utilize established methodologies and models to compute science yields (Krist et al. 2016, Traub et al. 2016).

The elements designed for M1a will be fabricated at JPL's Micro Devices Laboratory (MDL), at our dedicated vacuum deposition system, or an outside vendor as appropriate. These elements will be fabricated with known and proven methods (Trauger et al. 2010, 2011, 2016), minimizing cost and risks. We will evaluate the optical characteristics of these masks in the General Purpose Coronagraph Testbed (GPCT), a new vacuum coronagraph testbed in the JPL HCIT facility. Following successful development and evaluation, these elements will be transferred to the DST for TRL 5 demonstration of the performance predicted for M1a (cf. Table 1-1).

Once the LUVOIR configuration has been defined (expected during the first year of this study), including segment dimensions, optical characteristics, segment separations, and secondary mirror obscurations, then we will seek the best exoplanet performance as scored against our model for science yield of potential Earth-sized exoplanets among a representative population of nearby stars. WFIRST/CGI was an initial exploration of this design space, but now we will include a more complex pattern of pupil obscurations and panel misalignments.

Expected performance levels will be determined during the design phase of *M2a* (cf. Table 1-1). Masks will be fabricated and transferred to the DST. WFIRST/CGI was an initial exploration of this design space, but now we will include a more complex pattern of pupil obscurations and panel misalignments.

The following sections describe the testbed facilities.

4.1 The General Purpose Coronagraph Testbed (GPCT)

GPCT was constructed in 2017 for testing innovative coronagraph technologies. It resides in the HCIT-2 vacuum chamber, which will also host DST (see **Figure 3**). It is currently in operation to support another SAT-TDEM funded task (PI: Dr. Eugene Serabyn), demonstrating starlight suppression of broadband vector vortex masks. **Figure 4** depicts the GPCT setup. GPCT utilizes a super-continuum, white-light source with a tunable spectral band-pass filter. As such, it can deliver light centered at wavelengths ranging from 400 to 840 nm with 10 – 100 nm bandwidth (2% - 18% at λ = 550 nm). An

ultrathin precision circular pinhole made by MDL defines the optical source point. Six off-axis parabolic reflectors (OAPs) form the backbone of the optical train. OAP1 collimates the Source light to simulate starlight incident on a telescope pupil. A deformable mirror (DM) defines the pupil and redirects light toward OAP2, which produces a focal plane hosting a coronagraph mask. OAP3 collimates the beam to form a pupil conjugate for hosting a Lyot stop. OAP4 re-focuses the beam to form an image conjugate, which can host a field stop. Finally, OAP5 and OAP6 magnifies and projects the coronagraph image onto the camera. GPCT currently utilizes a 1024-actuator (32x32) DM from Xinetics. In the first quarter of calendar-year 2018, a 925-actuator DM from Boston MicroMachines will replace this DM for performance validation in an actual coronagraph. Computer-controlled actuations allow *in vacuo* swapping of focal-plane masks, Lyot stops, and projection of either the pupil or focal-plane images (via insertion/removal of a lens) onto the camera.

Our baseline plan utilizes GPCT for preliminary tests to reduce demand on DST. We will gain experience and knowledge, feeding into a design iteration, before entering DST for each of M1b and M2b. DST schedule permitting, we prefer to conduct all of our tests in the DST (bypassing the GPCT), as that would be more effective than learning in a different (GPCT) environment. We will coordinate with the ExEP program office to explore this option.

4.2 Decadal Survey Testbed (DST)

The DST is being constructed as a platform for contrasting different telescope apertures and coronagraph architectures, thereby advancing coronagraph state-of-the-art. Its main objective is to improve the chances that a direct-imaging, exoplanetary mission will be recommended by the 2020 Astrophysics Decadal Survey. Its implementation comprises three phases (Patterson et al. 2017):

- Phase I – Commissioning (clear, unobscured pupil; static demonstration): Using a Hybrid Lyot Coronagraph architecture with an unmasked circular pupil, demonstrate a 360º annular dark hole from 3 to 9 λ/D in a 10% bandpass centered at 550 nm with mean contrast ≤ 10^{-10}.
- Phase II – Segmented Telescope (segmented, obscured pupil; static demonstration): Using a TBD coronagraph, add a TBD segmented pupil mask and demonstrate a 360º annular dark hole from 3 to 9 λ/D in a 10% bandpass centered at 550 nm with mean contrast ≤ $5x10^{-10}$ (TBR).
- Phase III – Segmented Telescope (segmented, obscured pupil, dynamic demonstration): Same as Phase II, but now with a segmented telescope simulator and a disturbance source.

The completion of Phase I is planned for December, 2018. **Figure 5** depicts DST's optical layout. Compared to the GPCT, DST adds a second DM with one of the DMs mounted on a steering fixture, and LOWFS system. In addition to the FSDM for image stabilization and jitter injection, the DST elements will be better characterized and modeled, the DST bench will have better stability (e.g., low CTE carbon fiber bench, first mechanical resonance > 200 Hz, DM thermal control), and will include provisions for both HabEx and LUVOIR pupils. The design includes the following features:

- Pinhole light source illuminating an f/30 beam.
- One Fast/Fine Steering Deformable Mirror (FSDM) located at a system pupil, to stabilize the star at the center of the FPM. Driven by a typical commercial driver, the

steerable mirror can inject either static pointing offsets or rapid pseudo-random pointing sequences. This steerable element therefore provides a method to simulate telescope line-of-sight pointing errors and jitter. Further, the well-calibrated DM enables the open-loop addition of low-order zernike errors (z4-11) at a system pupil, providing a method to simulate telescope thermal drift. The DM will have 2304 (48x48) actuators.

- One Deformable Mirror (DM) in a static mount located downstream of the system pupil. The DM will also have 2304 (48x48) actuators.
- Three moveable coronagraph mask assemblies (occulter, Lyot stop, fieldstop)
- Telecentric design with selectable lens for accessing the pupil at the DICam (Direct Imaging Camera) plane.
- LOWFS (low order wavefront sensing) camera and control system provides low order (z2-z11) measurements to sense image jitter and wavefront drift at speeds up to 500 Hz.
- Direct Imaging Camera – captures images of the high-contrast dark field and enables high-order wavefront sensing.

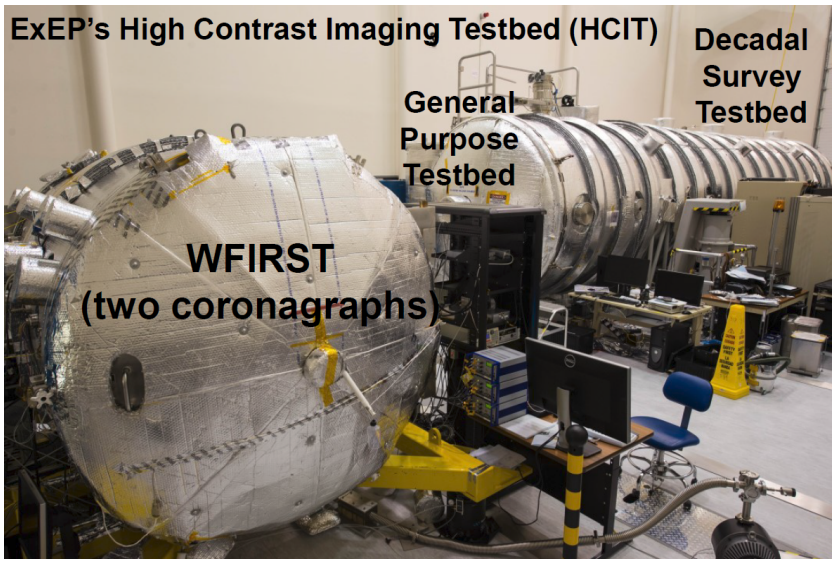

Figure 3. Layout of the current HCIT testbeds. The Decadal Survey Testbed, to be located in the west end of the large vacuum chamber, will be available for the SLEEC milestone demonstrations. Photo taken from Crill (2017).

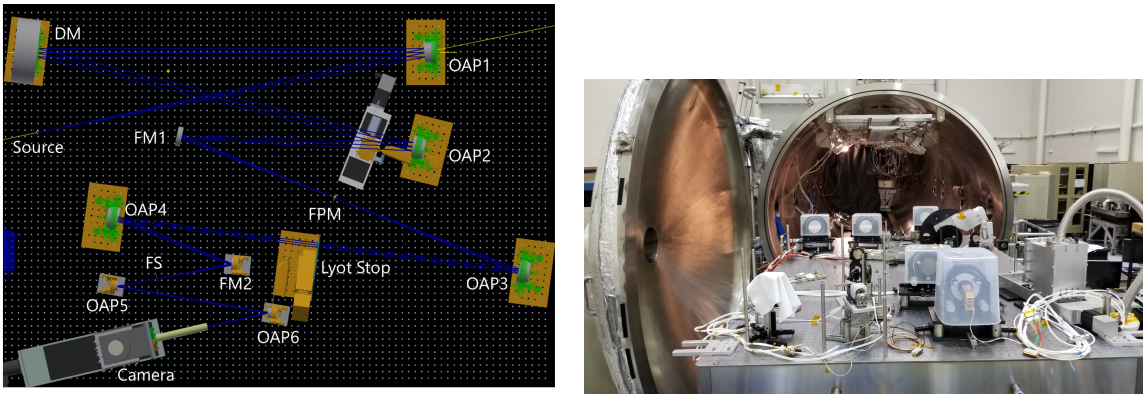

Figure 4. (Left) GPCT optical layout. DM: deformable mirror; OAPx: off-axis parabolic reflectors; FMx: fold mirrors; FPM: focal-plane mask. See body text for detailed description. (Right) Photograph of the actual GPCT testbed entering the HCIT-2 vacuum chamber.

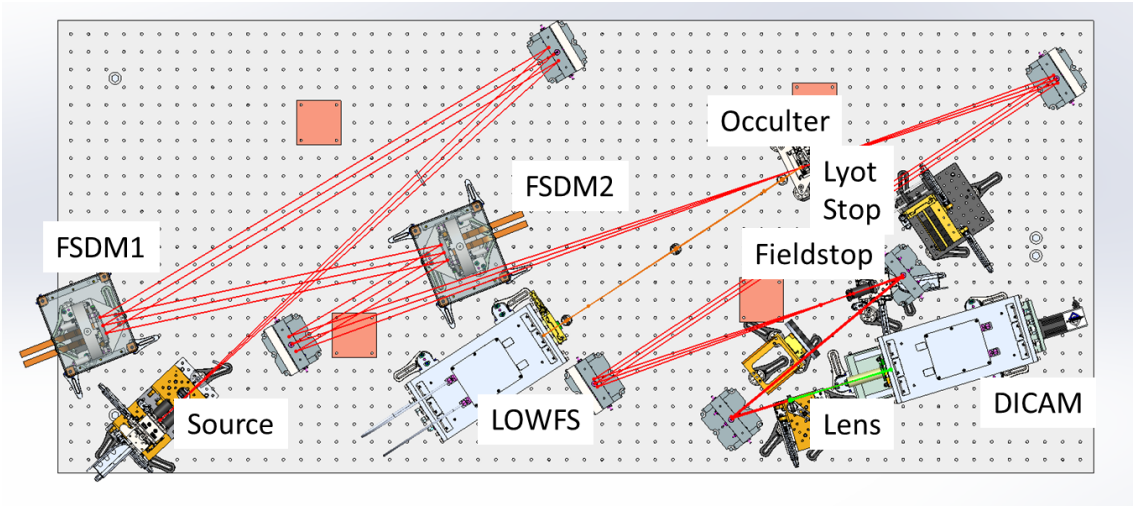

Figure 5. DST layout. FSDM1: fine-steering deformable mirror; FSDM2: deformable mirror in a static mount; LOWFS: low-order wavefront sensor; DICam: direct-imaging camera at the high contrast image plane.

5 Data Measurement & Analysis

In brief, a contrast measurement is a measurement of the intensity of the residual light (speckles, diffracted starlight, etc.) within the dark field, relative to the peak intensity of an image of the source/star. There is a distribution of intensities across the dark hole, from which the average contrast and its statistical confidence level is calculated. The milestone objective is to demonstrate with high confidence ($\geq 90\%$) that the true contrast in the dark field, as estimated from our measurements in the presence of noise, is equal to or better than the required threshold contrast, $c_0 = 1.0 \times 10^{-10}$.

Because of laboratory instabilities and the ongoing wavefront control algorithm, the contrast at any point in the dark field is time dependent, and so multiple successive exposures of the dark hole will be taken. For each image (where "each image" can itself be more than one sequential image if temporal averaging is deemed important to build up signal to noise), we calculate a spatial median/average of the measured contrast level over the

entire dark hole. This yields a series of m (with m required to be ≥ 4) individual dark-hole images, each with its own spatially averaged dark-hole contrast, c_i. We then take the mean over the series of m dark-hole images, leading to a sample-averaged contrast and variance, both defined below. Finally, we note that the entire experimental run is then to be repeated from scratch at least three times, to show repeatability. No averaging is done over the independent runs, so that the milestone is achieved independently n times.

As mentioned, the measured contrast is time dependent, being subject to laboratory conditions such as the quality of the optical components, their alignment, drifts in their alignment over time, and the effectiveness of each wavefront sensing and control cycle. With each iteration, our nulling procedure attempts to improve the contrast, thus compensating for any drift or alignment changes that may have occurred since the previous iteration. Further variations may be expected due to experimental noise and any limitations in the algorithm. The images built up from a sequence of such iterations will provide a distribution of contrast values, which will be regarded as Gaussian about a mean contrast for the data set. We therefore consider the mean contrast value as representative of the true contrast value for a given data set.

The contrast measurements of the iterations within a single run will fluctuate due to random measurement noise and wavefront control errors and drift. The statistical confidence level will thus require an estimation of the variance. Given that our speckle fields contain a mix of static and quasi-static speckles (the residual light field remaining after the completion of a wavefront sensing and control cycle, together with the effects of alignment drift following the control cycle), as well as other sources of measurement noise including photon detection statistics and CCD read noise, an analytical development of speckle statistics is impractical. Hence, we will compute the confidence coefficients on the assumption of Gaussian statistics. The full set of measurement will also be stored, to enable computation of the confidence levels for other statistics.

The following paragraphs define the terms involved in the measurement process, spell out the measurement steps, and specify the data products.

5.1 Definitions

5.1.1 Raw and Calibrated Image

Standard techniques for the acquisition of CCD images are used. A "raw" image is the pixel-by-pixel image obtained by reading the charge from each pixel of the CCD, and amplifying and sending it to an analog-to-digital converter. A "calibrated" image is a raw image that has had background bias subtracted and the detector responsivity normalized by dividing by a flat-field image.

5.1.2 Scratch

"Scratch" is a DM setting to a surface figure that is nominally flat with a predetermined average actuator voltage. It is understood that the DMs have been calibrated in advance such that the individual actuator influence functions, actuator gains (surface displacement/volt), and DM voltage settings for nominal flat surface figure are known. Since the high-contrast DM settings are close to the nominal flat setting, starting from scratch keeps the DM voltage transitions to a minimum and assures minimum DM actuator drift, which might otherwise complicate the contrast demonstration.

5.1.3 Algorithm

The "algorithm" is the computer code that takes as input the measured speckle field images, and produces as output a voltage value to be applied to each element of the DM, with the goal of reducing the intensity of speckles.

5.1.4 Star

The "star" is a small pinhole illuminated with broadband light relayed via single-mode optical fiber from a source outside the vacuum wall (e.g., a filtered super-continuum white light source). The "small" pinhole is to be unresolved by the optical system; e.g., a 3-μm diameter pinhole would be "small" and unresolved by the 16-μm FWHM Airy disk in an f/30 beam at 550 nm wavelength. This "star" is the only source of light in the optical path of the testbeds. It is a stand-in for the star image that would have been formed by a telescope system.

5.1.5 Contrast Field

The "contrast field" is a dimensionless map representing, for each detector pixel, the ratio of its value to the value of the peak of the PSF that would be measured in the same testbed conditions (light source, exposure time, Lyot stop, etc.) if the FPM were offset. The calibration of the contrast field is discussed in Section 5.3.

5.1.6 Median Contrast

The "median contrast" c_i is a dimensionless quantity that is, for a given image, the spatial median value of the contrast field over the defined dark hole.

5.1.7 Mean Contrast

The "mean contrast", $\hat{c}$, of a given sequence of $n \geq 4$ images is the mean of the individual average contrast values occurring in that sequence:

$$\hat{c} = \frac{1}{n}\sum c_i.$$

5.1.8 Milestone Metric

The mean contrast $\hat{c}$ is the variable whose value shall reach those stated in the milestone metrics.

5.1.9 Standard Deviation

The standard deviation σ_{meas} for an individual measurement of the average contrast value c_i is given as usual by:

$$\sigma_{meas} = \sqrt{\sum_{i=1}^{n} \frac{(c_i - \hat{c})^2}{n-1}}$$

The uncertainty in the mean contrast $\hat{c}$ is then given by

$$\sigma_{mean} = \frac{\sigma_{meas}}{\sqrt{n}}.$$

There is also a contribution to the uncertainty from the independently-determined photometry error, σ_{phot}. The net standard deviation is thus

$$\sigma = \sqrt{\sigma_{mean}^2 + \sigma_{phot}^2}$$

5.1.10 Statistical Confidence

We assume that contrast values from a set of iterated contrast measurements have a Gaussian distribution about the mean contrast. A dataset generally approaches the Gaussian distribution only when the number of data points become large (approaches infinity), even if the process underlying measurement errors are truly Gaussian. For small datasets (when n is less than about 20) one should use the Student's t-distribution to estimate confidence intervals. For a given confidence level, the t-distribution yields an interval of the following significance: if a large number of measurement trials were conducted, the large set of mean values from these trials would have a fraction of its members whose values fall within the interval, and this fraction is equal to the confidence level. The size of the interval is a function of sample size, and common t-distribution tables provide interval sizes indexed by confidence levels and sample sizes. As an example, for $n = 4$ at 90% (one-sided) confidence level, the interval is 1.638σ: in other words, for a sample of four contrast measurements, if the same measurement were repeated a large number of times and the errors are Gaussian random, 90% of the mean contrast values would be below $\hat{c} + 1.638\sigma$. Hence, we set $\hat{c} = c_0 - t\sigma$; meeting a milestone contrast target c_0 with the desired confidence level requires the final measured mean contrast $\hat{c}$ for a given run to be lower than the target contrast c_0 by t standard deviations. Thus, for 90% confidence and a sequence of *four* measurement runs, the following condition must be satisfied to meet milestone metrics: $\hat{c} \leq c_0 - 1.638\sigma$. If more data points are available, then t decreases.

5.2 Measurement of the Star Brightness

1. The FPM is displaced laterally relative to the center of the beam by approximately 6 λ/D, so as to transmit maximum stellar flux.
2. To create the photometric reference, a representative sample of short-exposure (e.g. a few milliseconds) images of the star is taken, with all coronagraph elements other than the FPM in place.
3. The images are averaged to produce a single star image. The "short-exposure peak value" of the star's intensity is estimated. As the camera pixels provide good sampling of the star image, the star intensity can be estimated using either the value of the maximum-brightness pixel or the peak brightness of a PSF profile fitted to the data.
4. The "peak count rate" (counts/sec) is measured for exposure times of microseconds to tens of seconds.

5.3 Measurement of the Coronagraph Dark Hole Contrast Field

1. The FPM is centered on the star image.
2. An image (typical exposure times are about 10s of seconds) is acquired of the coronagraph field (the suppressed star and surrounding speckle field). The dimensions of the high-contrast dark field are shown schematically in **Figure 6**. The 360° dark field extends from IWA= 3 λ/D to OWA = 10 λ/D in angular distance from the star for a two-DM testbed (e.g. DST).
3. The image is normalized to the "star brightness" as defined in 5.2, using the fixed ratio between peak star brightness and the integrated light in a region of the speckle field outside the central DM-controlled area; i.e., $\frac{dark\ hole}{star} = \frac{dark\ hole}{speckle} * \frac{speckle}{star}$. For this purpose, any well-defined region of the outer speckle field can be used; e.g., the red

region in **Figure 6**. To avoid saturation issues with the full-flux image case, there are usually three ratios involved:

a. Dark hole pixel/distant speckle field (both obtained with the FPM in)
b. Distant speckle field/inner point spread function (out to several Airy rings; both obtained with FPM out]
c. Inner point spread function/central point spread function pixel (both with FPM out). In our previous TDEM work, we found the distant speckle field to be unchanged by the insertion or removal (by lateral translation) of the FPM, thus providing a robust calibration ladder. Other calibration ladders may also be possible.

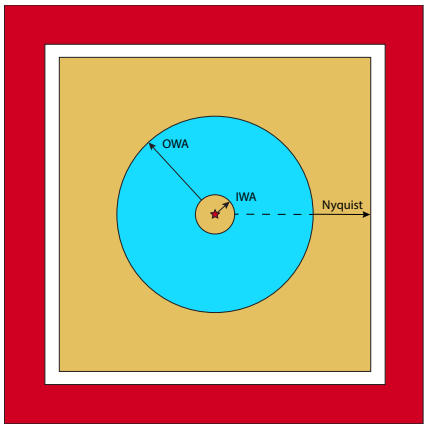

Figure 6. Definition of the target high-contrast dark field. The occulted star is at the center of the diagram. A 360° high contrast dark field (in blue) extends from the inner working angle (IWA) to the outer working angle (OWA). The speckle control region (in yellow) is square and extends to the Nyquist limit (angular distance from the star to the nearest side = $N\lambda/2D$, where N = actuator count across the DM). The reference field for contrast photometry (in red) is an area of uncontrolled speckles beyond the Nyquist boundaries.

5.4 Milestone Demonstration Procedure

Each laboratory demonstration consists of the following sequence:

1. The DM is set to a nominal flat surface ("scratch") at the chosen bias voltage. An initial coronagraph contrast field image is obtained as described in Section 5.3.
2. Wavefront sensing and control is performed to find settings of the DM actuators that give the required high-contrast in the target dark field. This iterative procedure may take several hours if no prior information is available.
3. A number of contrast field images are taken, following steps 1 – 2. A sufficient number (≥ 4) of images are taken to provide statistical confidence that the milestone contrast levels have been achieved, as described in Section 5.1.
4. Laboratory data are archived for future reference, including all raw images of the reference star and contrast field images.

5.5 Milestone Data Package

The milestone certification data package will contain the following:

1. A narrative report that includes a discussion of how each element of the milestone was met, with a narrative summary of the overall milestone achievement and its repeatability.
2. A description of the optical elements, including the FPMs, and their significant characteristics.
3. A tabulation of the significant operating parameters of the apparatus.
4. A contrast field image representative of the data set, with appropriate numerical contrast values indicated, with coordinate scales indicated in units of Airy distance (λ/D).
5. A description of the data reduction algorithms, in sufficient detail to guide an independent analysis of the delivered data.
6. Average and mean contrast values and standard deviations for the data used to satisfy the milestone requirements, including a pixel-by-pixel histogram of contrast values across the dark field.
7. For each image reported as part of the milestone demonstration, the average contrast within the annular area spanning 3-4 λ/D.

6 Success Criteria

The following are the required elements of the milestone demonstration. Each element includes a *brief rationale*.

1. Illumination is 10% bandwidth light in single or dual polarization at a wavelength in the range of 500 nm $< \lambda <$ 1000 nm. *Rationale: This milestone is an initial demonstration of the feasibility of the approach at a wavelength in the science band of Habex/LUVOIR.*
2. Coronagraph performance as stated in Section 3 shall be demonstrated. *Rationale: This provides evidence that the high contrast field is sufficiently dark to be useful for searching planets, and to carry out initial tests at small angles.*
3. Criterion 2 shall be met with a confidence of 90% or better. Sufficient data must be taken to justify this statistical confidence. *Rationale: Assuming the contrasts have a Gaussian distribution about the mean, this demonstrates a statistical confidence of 90% that the contrast goal has been met.*
4. Elements 1 – 3 must be satisfied on 3 separate occasions with a reset of the wavefront control system software (DM set to the initial flat setting) between each demonstration. *Rationale: This provides evidence of the repeatability of the contrast demonstration. The wavefront control system software reset between data sets ensures that the different data sets can be considered as independent and do not represent an unusually good configuration that cannot be reproduced. There is no requirement on the duration of these experiments or the interval between demonstrations. There is also no requirement to turn off power, open the vacuum tank, or delete data relevant for the calibration of the DM influence function*

7 Schedule

7.1 Nominal Work Plan

The technology development work officially commences upon the approval of this white paper, assumed to occur at the end of the first quarter (Q1) in calendar year 2018. We begin this work by designing the HabEx (M1a/b) coronagraph. By the end of Year 1 (2018), we will complete detailed fabrication drawings and specifications for necessary masks and

apodizers; this enables component fabrications at the beginning of Year 2. We conclude Year 1 with the submission of the M1a Report.

Year 2's main thrust is achieving M1b: validation of our HabEx coronagraph performance. This encompasses fabrication and acquisition of necessary components, preliminary tests, a design iteration, and full validation in the DST.

We now expect the DST to be operational prior to the beginning of Year 2. We prefer to proceed immediately to the DST demonstration if compatible with the DST schedule, thus bypassing the GPCT setup, as this would save time and eliminate duplicated efforts. We will apply for DST testbed time, with the objective of completing M1b in Year 2. Past TDEM experience indicates that the commissioning of a new coronagraph configuration may take as long as 3 months. New coronagraph elements will be characterized in the commissioning period. Any anomalies will be analyzed and remedies devised, including additional fabrication runs at the MDL if required (with an estimated 3-month turn-around). The milestone demonstrations to be carried out in a subsequent 3-month period.

A parallel line of work in Year 2 comprises our LUVOIR coronagraph design. This leads to detailed drawings and specifications for masks and apodizers, as well as the M2a Report in the first quarter of Year 3. We will complete M2a in Year 3. We will complete M2b in Year 3.

Year-3's main thrust is achieving M2b: validation of our LUVOIR coronagraph performance. This encompasses fabrication and acquisition of necessary components, preliminary tests, a design iteration, and full validation in the DST. We will apply for DST testbed time and complete M2b in Year 3. We will submit the M2b report by the end of Year 3.

We have discussed the proposed DST plans with appropriate ExEP authorities and obtained mutually compatible understanding. We will coordinate with HCIT management (Dr. Hong Tang) to schedule testing in the GPCT.

Figure 7 shows the schedule plan of major activities and milestones.

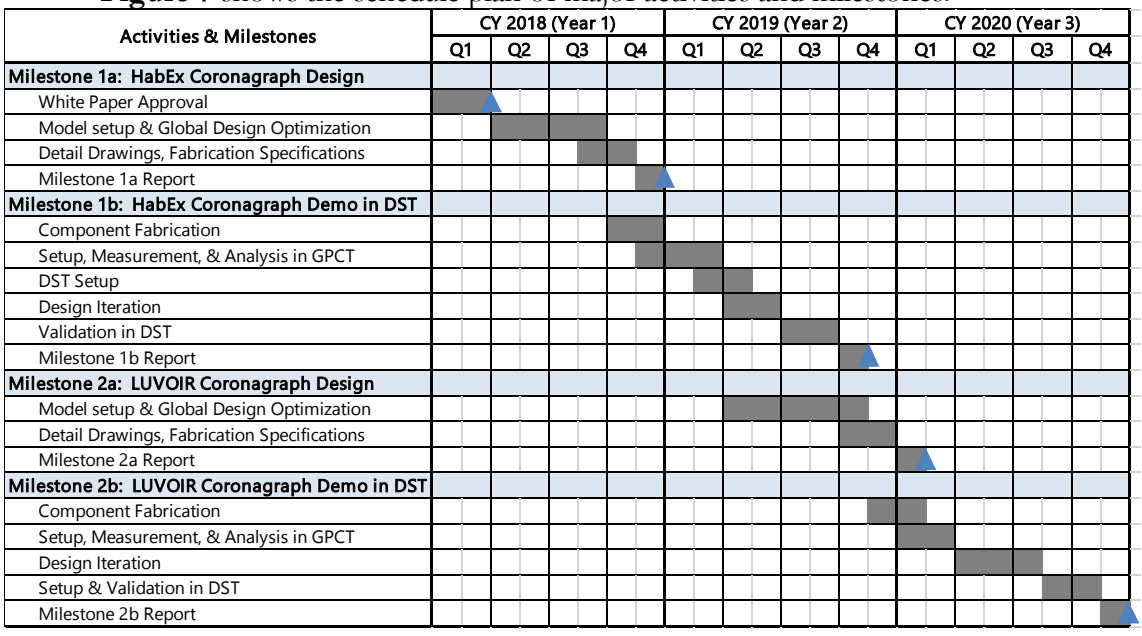

Figure 7. Schedule of major activities and key milestones

7.2 Schedule Risks and Mitigation

7.2.1 DST Schedule

The DST team currently plans for DST first light in vacuum in April, 2018, with dark-hole digging using a preliminary mask commencing in June, 2108. Our nominal schedule is commensurate with the current DST schedule. Our team members are directly involved with DST work. This greatly facilitates continual coordination with DST to minimize implementation risk.

7.2.2 Uncertainty of the LUVOIR Pupil Architecture

At this time, the LUVOIR design team has not fully converged on a pupil architecture. Our design and performance objectives depends on this convergence, and we rely on our experience and technical capabilities to anticipate design possibilities and maintain agility to mitigate risk. Once the LUVOIR design reaches sufficient resolution, we will submit a white-paper addendum for TAC approval.

7.3 Team Members and Other Key Personnel

John Trauger, the Principal Investigator, will manage the task and direct the research effort, keeping foremost the ultimate goal of advancing technology readiness for HabEx and LUVOIR exoplanet imaging and spectroscopy. He brings his knowledge of exoplanet science objectives, the essential elements of the actively-corrected space coronagraph, as well as his background in multilayer thin film design and fabrication. In particular, he will be in charge of mask fabrications and coronagraphic performance validations.

Pin Chen, Co-Investigator, will be intimately involved in all aspects of this task. He brings his experience in the development and delivery of laboratory and flight optical systems. He is the developer of the herein described MCMC approach to coronagraph design. He will take the lead in the overall design optimization effort.

Dwight Moody, Co-Investigator, has developed our gradient-guided design optimization algorithms and wavefront-control software. He will use his integrated code to explore advanced mask design options and prepare deposition prescriptions for the physical realization of the masks. He will also apply these same codes to the operation of the CCDF wavefront control systems.

John Krist, Co-Investigator, brings his expertise in optical modeling to analyze and tolerance the coronagraph performance design and to evaluate the science performance/impact of various coronagraph design trades.

We will utilize MDL's fabrication capabilities for mask/apodizer fabrications through JPL's infrastructure service system. We have extensive relevant experience in working with MDL to produce coronagraph components.

In addition, HCIT/DST technical staff will provide necessary support. The following is an excerpt from the ExEP's letter of support for the proposal associated with the herein described work:

> "Should your proposal be awarded, ExEP will commit to providing the requested DST testbed time, making a best effort to schedule at an agreeable time your use of DST, in coordination with other funded users of the testbed. The testbed provided by ExEP will include a coronagraph compatible with your drop-in masks; no additional specialized hardware was requested. In addition, ExEP will commit to providing personnel to assist

with hardware integration, optical alignment, and software integration at no cost to your award, if selected."

8 References

Belikov, R., N. J. Kasdin, and R. J. Vanderbei (2006), Diffraction-Based Sensitivity Analysis of Apodized Pupil Mapping Systems, ApJ, 652, 833–844.

Carlotti, A., Pueyo, L., and Mawet, D. (2014), "Apodized phase mask coronagraphs for arbitrary apertures II. Comprehensive review of solutions for the vortex coronagraph," A&A, 566, doi: 10.1051/0004-6361/201323258.

Crill, B. P. & N. Siegler (2017), Space Technology for directly imaging and characterizing exo-Earths, Proc. SPIE 10398, doi: 10.117/12.2275697

Foreman-Mackey, D., D. W. Hogg, D. Lang, and J. Goodman (2013), emcee: The MCMC Hammer, Publications of the Astronomical Society of the Pacific, 125, 306–312.

Guyon, O. (2003), Phase-induced amplitude apodization of telescope pupils for extrasolar terrestrial planet imaging, Astronomy and Astrophysics, 404(1), 379–387.

Jensen-Clem, R., et al. (2018), "A New Standard for Assessing the Performance of High Contrast Imaging Systems," Ap.J., 155, 19.

Kasdin, N. J., R. J. Vanderbei, D. N. Spergel, and M. G. Littman (2003), Extrasolar Planet Finding via Optimal Apodized-Pupil and Shaped-Pupil Coronagraphs, ApJ, 582(2), 1147–1161.

Krist, J. E. (2007), PROPER: an optical propagation library for IDL, in Proceedings of SPIE Vol. 6675, Optical Modeling and Performance Predictions III, edited by Mark A. Kahan.

Krist, J. E. (2016), Contrast Definitions for Direct Imaging of Extrasolar Planets, JPL document.

Krist, J., B. Nemati, and B. Mennesson (2016), Numerical modeling of the proposed WFIRST-AFTA coronagraphs and their predicted performances, JATIS 2(1), 011003.

Mawet, D., Serabyn, E., Liewer K., Burruss, R., Hickey, J., and Shemo, D. (2010), "The Vector Vortex Coronagraph: Laboratory Results and First Light at Palomar Observatory," Ap. J., 709, 53-57.

Mazoyer, J., Pueyo, L., Norman, C., N'Diaye, M., van der Marel, R. P., and Soummer, R. (Mar. 2016), "Active compensation of aperture discontinuities for WFIRST-AFTA: analytical and numerical comparison of propagation methods and preliminary results with a WFIRST-AFTA-like pupil," JATIS 2(1) , 011008.

Patterson K., ExEP HCIT DST Team (2017), Decadal Survey Testbed (DST) Peer Review, JPL document.

Papoulis, A. (1968), System and Transforms with Applications in Optics, McGraw Hill Book Co., New York

Pueyo, L., and C. Norman (2013), High contrast imaging with an arbitrary aperture: active compensation of aperture discontinuities, Ap.J., 769, 102–133.

Press, W. H., B. P. Flannery, S. A. Teukolsky, and W. T. Vetterling (1992), Numerical Recipes in FORTRAN 77: The Art of Scientific Computing, 2nd ed., Sec. 10.0, Cambridge University Press, Cambridge.

Seo, Byoung-Joon, et al. (2017), WFIRST project updates to performance data reported in Seo, B.-J., B. Gordon, B. Kern, A. Kuhnert, D. Moody, et al. (2016), Hybrid Lyot coronagraph for wide-field infrared survey telescope-astrophysics focused telescope assets: occulter fabrication and high contrast narrowband testbed demonstration, JATIS 2(1), 011019

Siegler, N. (2016), Exoplanet Exploration Program: Technology Plan Appendix, NASA Jet Propulsion Laboratory, California Institute of Technology

Slepian, D. & H.O. Pollak (1961), Prolate Spheroidal Wave Functions, Fourier Analysis and Uncertainty – I, The Bell System Technical Journal, 40(1), 43–63.

Slepian, D. (1964), Prolate Spheroidal Wave Functions, Fourier Analysis and Uncertainty – IV: Extensions to Many Dimensions, Generalized Prolate Spheroidal Functions, The Bell System Technical Journal, 43(6), 3009–3057.

Slepian, D. (1983), Some Comments on Fourier Analysis, Uncertainty and Modeling, SIAM Review 25(3), 379-393.

Soummer, R., L. Pueyo, A. Ferrari, C. Aime, A. Sivaramakrishnan, et al. (2009), Apodized Pupil Lyot Coronagraphs for Arbitrary Apertures. II. Theoretical Properties and Application to Extremely Large Telescopes, Ap.J., 695, 695-706.

Traub, W.A., J. Breckinridge, T.P. Greene, O. Guyon, N.J. Kasdin, and B. Macintosh (2016), Science yield estimate with the Wide-Field Infrared Survey Telescope coronagraph, JATIS 2(1), 011020.

Trauger, J. T., K. R. Stapelfeldt, W. A. Traub, J. E. Krist, D. Moody et al. (2010), ACCESS: a concept study for the direct imaging and spectroscopy of exoplanetary systems, in Proceedings of SPIE 7731, 773128.

Trauger, J. T., D. Moody, B. Gordon, J. E. Krist, and D. Mawet (2011), A hybrid Lyot coronagraph for the direct imaging and spectroscopy of exoplanet systems: recent results and prospects, in Proceedings of SPIE 8151, 81510G.

Trauger, J. T., D. Moody, J. E. Krist, and B. L.Gordon (2016), Hybrid Lyot coronagraph for WFIRST-AFTA: coronagraph design and performance metrics, JATIS 2(1), 011013

9 List of Acronyms

CGI: Coronagraph Instrument (onboard WFIRST)
CTE: coefficient of thermal expansion
DICam: direct imaging camera
DM: deformable mirror
DST: Decadal Survey Testbed
ExEP: Exoplanet Exploration Program
FPM: focal-plane mask
FSDM: fine-steering DM
GPCT: General Purpose Coronagraph Testbed

HabEx: Habitable Exoplanet Imaging Mission
HCIT: High Contrast Imaging Testbed
HLC: hybrid Lyot coronagraph
IWA: inner working angle
LOWFS: low-order wavefront sensor
LUVOIR: Large UV/Optical/IR Surveryor
M1a: milestone 1a
M1b: milestone 1b
M2a: milestone 2a
M2b: milestone 2b
MCMC: Markov Chain Monte Carlo
MDL: JPL Microdevices Lab
OAP: off-axis parabolic reflectors
OWA: outer working angle
PIAA: phase-induced amplitude apodization
PIAACMC: PIAA complex mask coronagraph
PSF: point spread function
PSWF: prolate spheroidal wave function
SLEEC: Super Lyot ExoEarth Coronagraph
SPC: shaped pupil coronagraph
SPLC: shaped pupil Lyot coronagraph
TAC: Technical Advisory Committee
TBR: to be resolved
TDEM: Technology Development for Exoplanet Missions
TRL: Technology Readiness Level
WFIRST: Wide Field Infrared Survey Telescope